

Artículo aceptado en / *Paper accepted in*

## REVISTA MEXICANA DE CIENCIAS GEOLÓGICAS



Versión preliminar / *Draft versión*

### **Mineralogical characterization of gold alluvial sands preconcentrates in the mining districts of Huepetuhe and Delta 1, Madre de Dios region, Peru**

por / *by*

**Daniel Merino, Mery Gómez, Kevin Telmer, Cesar Paccha**

© 2025 Los autores

<https://creativecommons.org/licenses/by/4.0/>



Artículo recibido: diciembre 20, 2024

Artículo corregido recibido: abril 2, 2025

Artículo aceptado: abril 2, 2025

Versión preliminar publicada: abril 3, 2025

# Mineralogical characterization of gold alluvial sands preconcentrates in the mining districts of Huepetuhe and Delta 1, Madre de Dios region, Peru

Daniel Merino<sup>1\*</sup>, Mery Gómez<sup>2</sup>, Kevin Telmer<sup>3</sup>, Cesar Paccha<sup>1</sup>

<sup>1</sup> PhD candidate, Facultad de Ingeniería Ambiental, Universidad Nacional de Ingeniería, Lima, 15333, Peru.

<sup>2</sup> PhD in Metallurgical and Materials Engineering, Universidad Nacional de Ingeniería, Lima, 15333, Peru.

<sup>3</sup> Artisanal Gold Enterprises Inc, Victoria BC, Canada.

\*Corresponding author (D. Merino): [daniel.merino.n@uni.pe](mailto:daniel.merino.n@uni.pe)

## ABSTRACT

Artisanal and small-scale gold miners (ASGM) in the Madre de Dios region use mercury for gold processing, making it the primary source of environmental contamination. However, the lack of geochemical and mineralogical characterization of alluvial preconcentrates limits the search for alternative metallurgical processes. To address this, seven samples of alluvial preconcentrates (CQI-04, CQI-05, DAI-01, DAI-02, DAI-03, DAI-29, DAI-Hg-06) from two mining concessions in the districts of Huepetuhe and Delta 1 were analyzed to determine their geochemical and mineralogical composition. The study included X-ray Fluorescence (XRF) and X-ray Diffraction (XRD), Optical Microscopy (OM), Scanning Electron Microscopy (SEM), and sieve analysis with fire assay for gold quantification. The Puerto Belén concession, located in the Huepetuhe district, contains more than 80% coarse gold particles (>250  $\mu\text{m}$ ) and is rich in iron oxides (ilmenite, magnetite, hematite), quartz, and minor amounts of andalusite, zircon, and unidentified phases containing light rare earth elements (LREE). The Raul 1 concession, in the Delta 1 district, has 50% medium-sized gold particles (106–250  $\mu\text{m}$ ), 28% fine gold (<106  $\mu\text{m}$ ), and 23% coarse gold (>250  $\mu\text{m}$ ), with dominant quartz content, followed by hematite, ilmenite, zircon, rutile, muscovite, and LREE-bearing phases. In both concessions, gold exhibits high purity (99% Au, 1% Ag). Optical and electron microscopy analyses reveal sub-rounded to elongated gold particles within ferritic and siliceous matrices. Understanding the geochemical and mineralogical

characteristics of alluvial preconcentrates is essential for proposing mercury-free metallurgical alternatives that enhance gold recovery and enable the extraction of other economically valuable minerals such as iron, titanium, zircon, and rare earth elements.

**Key words:** characterization; preconcentrate; benefit; gold; mercury; rare earth elements.

## RESUMEN

*Los mineros artesanales y de pequeña escala (ASGM, por sus siglas en inglés) en la región de Madre de Dios utilizan mercurio para el procesamiento del oro, lo que constituye una problemática ambiental. Sin embargo, la falta de caracterización geoquímica y mineralógica de los preconcentrados aluviales limita la búsqueda de procesos metalúrgicos alternativos. Para abordar esta problemática, se analizaron siete muestras de preconcentrados aluviales (CQI-04, CQI-05, DAI-01, DAI-02, DAI-03, DAI-29, DAI-Hg-06) de dos concesiones mineras en los distritos de Huepetuhe y Delta 1, con el objetivo de determinar su composición geoquímica y mineralógica. El estudio incluyó Fluorescencia de Rayos X (XRF) y Difracción de Rayos X (XRD), Microscopía Óptica (OM), Microscopía Electrónica de Barrido (SEM) y análisis granulométrico con ensayo al fuego para la cuantificación de oro. En la concesión de Puerto Belén, ubicada en el distrito de Huepetuhe, el oro ocurre en más del 80% en partículas gruesas (>250  $\mu\text{m}$ ), acompañadas de óxidos de hierro (ilmenita, magnetita, hematita), cuarzo y cantidades subordinadas de andalucita, circón y fases no identificadas con elementos de tierras raras ligeras (LREE, por sus siglas en inglés) c. La concesión Raúl 1, en el distrito Delta 1, tiene 50% de partículas de oro de tamaño medio (106–250  $\mu\text{m}$ ), 28% de oro fino (<106  $\mu\text{m}$ ) y 23% de oro grueso (>250  $\mu\text{m}$ ), con contenido dominante de cuarzo, seguido de hematita, ilmenita, circón, rutilo, moscovita y fases portadoras de LREE. En ambas concesiones, el oro presenta una alta pureza (99% Au, 1% Ag). Los análisis mediante microscopía óptica y electrónica revelan partículas de oro subredondeadas a elongadas dentro de matrices ferríticas y silíceas. La comprensión de las características geoquímicas y mineralógicas de los preconcentrados aluviales es fundamental para proponer alternativas metalúrgicas libres de mercurio que mejoren la recuperación del oro y permitan la extracción de otros minerales de interés económico, como hierro, titanio, circón y tierras raras.*

**Palabras clave:** caracterización; preconcentrado; beneficio; oro; mercurio; tierras raras.

## INTRODUCTION

Artisanal and small-scale gold mining (ASGM) is widespread across Peru, with alluvial and underground gold extraction occurring in all 24 regions. Approximately 95% of ASGM gold production is concentrated in Madre de Dios, Puno, Arequipa, Ayacucho, and Ica. ASGM in the Peruvian Amazon represents over 50% of the country's gold production, primarily from alluvial deposits (USAID, 2021; AGC, 2022). In alluvial ASGM operations, mineral preconcentrates contain not only gold but also other economically significant minerals, including iron oxides, titanium minerals, and minerals with rare earth elements (REE). However, the lack of detailed mineralogical characterization studies limits the ability to optimize beneficiation methods and explore the potential recovery of associated minerals (Mosquera et al., 2009; Osoreo et al., 2012; Velásquez, 2017). This study focuses on the mineralogical and geochemical characterization of alluvial gold preconcentrates from two mining concessions in the Madre de Dios region. To achieve this, optical microscopy (OM) and scanning electron microscopy (SEM) were employed to analyze the morphology and liberation of gold particles (Pirard, 2004; Chaves & Calixto, 2017). X-ray fluorescence (XRF) and X-ray diffraction (XRD) techniques were used to determine the elemental and mineralogical composition of preconcentrates, which is essential for assessing the presence of valuable minerals beyond gold (Wills & Finch, 2015; Gaspar, 2020). The granulometric distribution of gold was analyzed through particle size distribution (screening) to evaluate its implications for beneficiation processes (Frimmel, 2018), while fire assay testing, a standard method for quantifying gold content in mineral samples, was conducted to ensure accuracy in gold concentration measurements (Liu et al., 2019). Understanding the mineralogical composition of these preconcentrates is essential for optimizing beneficiation strategies, improving gold recovery, and evaluating the economic potential of other minerals present in the deposits. The findings from this study provide a foundation for assessing alternative processing methods and may contribute to a broader understanding of alluvial gold deposits in the Peruvian Amazon.

## **GEOLOGICAL SETTING**

### **Location**

The study area includes two mining concessions: Puerto Belén, located in the District of Huepetuhe, and Raul 1, situated in the Delta 1 Populated Center. Both concessions belong to the Province of Manu, within the Madre de Dios department, in southeastern Peru (Figure 1). Madre de Dios is part of the

Peruvian Amazon, bordering Brazil to the east and Bolivia to the southeast. The study area is approximately 300 km east of Cusco and 150 km southwest of Puerto Maldonado, the capital of Madre de Dios. The mining sites are located within the Amazonian lowlands, characterized by extensive river networks and alluvial deposits rich in gold. The Huepetuhe district and Delta 1 are among the most active mining zones in the region, where ASGM is the dominant economic activity. The Puerto Belén mining concession (INGEMMET Code: 070007900) is currently undergoing formalization and is owned by Mr. Damián Alfredo Ampuero Huaquisto. The Raul 1 concession (INGEMMET Code: 070007807) is held by Los Tres Emblemas Dorados de Oro S.A.C. The concessions lie within the Inambari River basin, an area characterized for its Quaternary alluvial deposits, which host significant gold mineralization derived from the erosion of the Andean Cordillera. The geographic coordinates of the study area, in UTM WGS84 Zone 19S, are approximately Easting: 347810.600, Northing: 8553628.060 for Puerto Belén; and Easting: 328810.210, Northing: 8577628.460 for Raul 1.

## Geology

The Quaternary alluvial deposits of the Madre de Dios region form part of the Amazonian plain, encompassing gold-bearing placer deposits associated with the Madre de Dios, Inambari, and Tambopata rivers (Valderrama, 2015). These deposits originate from the Eastern Cordillera, specifically from the sub-Andean Mountain range (piedmont), which is composed of Cretaceous and Tertiary sedimentary sequences. The main geological formations in this region are the Madre de Dios Formation and the alluvial deposits, along with the Mitu Group (Permo-Triassic) (INGEMMET, 2003). Locally, these units are overlain by alluvial deposits (Lanckneus, 1991). The sediments in this region are derived from the erosion of Andean terranes, leading to the formation of placer deposits, which can be classified into two main types: (1) residual deposits, which remain near their source rock, and (2) transported deposits, which have been relocated by fluvial processes (Prater, 1957) (Figure 2). The gold placers examined in this study belong to the Amazon hydrographic network. Specifically, the Puerto Belén mining concession is located within the Inambari River sub-basin, while the Raul 1 concession is within the Colorado River sub-basin, corresponding to the Masuco (27v) and Puerto Luz (26u) quadrangles, respectively. The lithostratigraphic units present in Puerto Belén include the Madre de Dios Formation (NQ-md), composed of gravel, sand, silt, clay, and minor conglomerates with iron oxides. Additionally, alluvial deposits (Qh-al) are present on the west bank of the Inambari River, consisting of poorly sorted gravels, sands, silts, and mica clays.

In the Raul 1 concession, the Madre de Dios Formation (NQ-md) is also present, containing Neocomian Red Layers, gray sands, and clays, along with alluvial terrace deposits (Qh-al), which consist of sands and gravels. The lithostratigraphic unit codes follow the stratigraphic classification of INGEMMET (1996).

## **Stratigraphy**

The sedimentary sequence of the Puerto Belén concession has been mapped and summarized in a generalized stratigraphic column (Figure 3). The base, between 390 and 430 m above sea level (a.s.l.), consists of a gravel sequence with matrix (GM), composed of angular and subangular pebbles and cobbles of andesite, granite, sandstone, gabbro, diorite, quartzite, and slate, which originate from the erosion of older geological units of the Eastern Cordillera, possibly associated with metamorphic and igneous formations of the region, interbedded with thin layers of sand and clay. Lenses of manganese oxides and the presence of hematite, limonite, jarosite, quartz, and mica stand out. The intermediate part, between 430 and 470 m a.s.l., is made up of gravel with clay matrix (GC), containing blocks, cobbles, and pebbles of volcanic composition such as rhyolite, and dacite, as well as carbonate rocks. This unit also presents sandy and silty sequences with the presence of iron oxides, jarosite, and small lenses of manganese oxides (pyrolusite), with calcite pore filling. The upper level, between 470 and 500 m a.s.l., consists of poorly sorted gravel (GP), composed mainly of boulders, pebbles, and to a lesser extent, sand and clays. The gravels are of igneous, sedimentary, and metamorphic origin, formed by andesite, dacite, granite, diorite, sandstone, quartzite, slate, gneiss, and carbonate rocks. Additionally, sporadic fossil logs, manganese oxide lenses, and a greater presence of hematite, limonite, and jarosite are observed. The intermediate and upper levels represent the prospective sequences currently being mined.

## **Mineralization**

The gold deposits of the Madre de Dios region are classified as alluvial placer deposits, formed by the erosion, transport, and deposition of gold-bearing materials derived from primary sources. These deposits occur in river terraces, floodplains, and active channels, where gold accumulates due to hydraulic sorting processes (Mosquera et al., 2009). Economic mineralization consists primarily of detrital gold particles (coarse, fine, and laminar) with low silver content, dispersed in gravel, sand, and clay. These particles are distributed horizontally across the main mining districts, including Huepetuhe, Inambari, Laberinto, Tambopata, and Madre de Dios (Merino et al., 2022). In addition to gold, the deposits contain

heavy minerals such as ilmenite ( $\text{FeTiO}_3$ ), hematite ( $\text{Fe}_2\text{O}_3$ ), magnetite ( $\text{Fe}_3\text{O}_4$ ), zircon ( $\text{ZrSiO}_4$ ), and epidote ( $\text{Ca}_2(\text{Al,Fe})_3(\text{SiO}_4)_3(\text{OH})$ ) (Lanckneus, 1989; Medina, 1999; INGEMMET, 2003). Accessory minerals include beryl ( $\text{Be}_3\text{Al}_2\text{Si}_6\text{O}_{18}$ ), monazite ( $(\text{Ce,La,Nd,Th})\text{PO}_4$ ), corundum ( $\text{Al}_2\text{O}_3$ ), and garnets ( $(\text{Fe,Mg,Ca,Mn})_3\text{Al}_2\text{Si}_3\text{O}_{12}$ ) (Aranda, 1999). Additionally, river sediments in the region also host REE minerals. Monazite concentrations of 4.7% have been reported in the Malinowsky River, 2.2% in the Tambopata River, 0.9% in the Madre de Dios River, and 0.8% in the Lower Inambari River (Lanckneus, 1991). In the Huepetuhe and Caychive river basins, within the Province of Manu, gold recovery processes produce black sands that contain REE, along with significant amounts of titanium and zirconium (Medina, 1999).

## METHODOLOGY

The mineralogical characterization was carried out on samples obtained from the washing of carpets in two mining concessions located in the districts of Huepetuhe and Delta 1, Madre de Dios. These samples correspond to preconcentrates of alluvial gold sands. The preconcentrate samples were labeled CQI-04, CQI-05, DAI-01, DAI-02, DAI-03, and DAI-29, while a mercury-contaminated preconcentrate (black sands) was designated as DAI-Hg-06 (Table 1). Mineralogical and geochemical analyses were performed using X-ray diffraction (XRD), X-ray fluorescence (XRF), optical microscopy (OM), and scanning electron microscopy (SEM) at BIZAlab S.A.C.

The XRD analysis was conducted using a PANalytical X'Pert PRO diffractometer equipped with a Co tube (35 kV, 30 mA), operating with K-alpha1 ( $\lambda = 1.78897 \text{ \AA}$ ) and K-alpha2 ( $\lambda = 1.79285 \text{ \AA}$ ) radiation. The measurement range was set from  $2\theta = 6^\circ$  to  $2\theta = 75^\circ$ . Calibration was performed using a silicon standard to ensure accuracy, with periodic recalibrations to minimize systematic errors. Mineral quantification was carried out using the AMCSD (American Mineralogist Crystal Structure Database).

For XRF analysis wavelength-dispersive X-ray fluorescence spectrometer (WDXRF) was used under a controlled temperature of  $24^\circ\text{C}$ , employing scintillation and flow counter detectors. Optical microscopy (OM) was conducted using an OLYMPUS BX-53 microscope under reflected and transmitted light conditions. The quantitative mineral content obtained from petrographic analysis is expressed in

modal percentage (% modal). Scanning electron microscopy (SEM) analyses were performed with a TESCAN XMU second-generation microscope, providing high-resolution imaging and elemental analysis.

Valued Mesh tests were carried out at the Mineral and Materials Processing Laboratory (Lab #10) of the Professional School of Metallurgical Engineering (EPIM), Faculty of Geological, Mining, and Metallurgical Engineering (FIGMM) at the National University of Engineering (UNI) and at the Silver Metallurgy S.A.C. (METASIL) plant. Fire assay tests for gold (AuFFAA) were conducted at the CJV S.A.C. laboratory, while ICP analyses were performed at the ALS Peru S.A. laboratory. All tests were conducted under controlled conditions with rigorous quality control procedures to ensure the reliability of the results. A detailed summary of the analyses performed on each sample is provided in (Table 1).

## RESULTS

The results of the various tests used for mineralogical characterization are shown below.

### Geochemistry

#### *X-ray fluorescence*

The XRF analysis of sample DAI-02 reveals a composition of 50.04% iron oxides, 23.18% silica, 14.84% titanium, 7.05% aluminum, 1.83% zirconium, and 3.06% minor oxides (including vanadium, manganese, tin, potassium, magnesium, cerium ( $\text{CeO}_2$ ), niobium, phosphorus, yttrium ( $\text{Y}_2\text{O}_3$ ), copper, and zinc) (Figure 4A). Sample DAI-Hg-06 contains 49.41% iron oxides, 21.61% silica, 19.73% titanium, 5.14% aluminum, 1.85% zirconium, and 2.26% minor oxides (manganese, vanadium, potassium, tin, magnesium, niobium, yttrium (Y), phosphorus, and zinc) (Figure 4B). Sample CQI-04 is dominated by 42.28% silica, 23.00% iron, 18.82% titanium, 8.48% zirconium, 2.94% aluminum, and 4.47% minor oxides (manganese, cerium ( $\text{CeO}_2$ ), vanadium, neodymium ( $\text{Nd}_2\text{O}_3$ ), potassium, lanthanum ( $\text{La}_2\text{O}_3$ ), hafnium, phosphorus, tungsten, magnesium, yttrium (Y), niobium, and zinc) (Figure 4C) (Table 3).

#### *X-ray diffraction*



The XRD analysis of sample DAI-02 indicates a mineralogical composition of 25% ilmenite, 23% magnetite, 22% hematite, 18% quartz, 3% andalusite, 3% muscovite, 2% zircon, and 1% other minerals (including rutile, goethite, chlorite, and cassiterite) (Figure 5D). Sample DAI-Hg-06 consists of 28% quartz, 25% ilmenite, 19% hematite, 18% magnetite, 3% andalusite, 2% zircon, and 5% other minerals (kaolinite, rutile, and muscovite) (Figure 5E). Sample CQI-04 is primarily composed of 55% quartz, 15% ilmenite, 11% zircon, 9% hematite, 3% rutile, 2% muscovite, and 5% other minerals (kaolinite, andalusite, and monazite (Ce,La,Nd)PO<sub>4</sub>) (Figure 5F) (Table 3).

### ***Inductively Coupled Plasma Mass Spectrometry***

The ICP-MS analysis of samples DAI-29 and DAI-03 reveals the presence of light REE, specifically cerium (Ce) and lanthanum (La), with concentrations exceeding 500 ppm and 260 ppm, respectively. Additionally, heavy REE such as yttrium (Y) were detected, with anomalies of 29.8 ppm, along with thorium (Th) anomalies reaching 50.4 ppm (Figure 6) (Table 3).

### **Petrography**

Petrographic analysis using reflected and transmitted light microscopy was conducted on samples DAI-02 and CQI-04.

#### ***DAI-02 sample***

The mineralogical composition of the DAI-02 sample consists of over 70% iron oxides, including magnetite (Fe<sub>3</sub>O<sub>4</sub>), ilmenite (FeTiO<sub>3</sub>), and hematite (Fe<sub>2</sub>O<sub>3</sub>). Magnetite (38%) is present as particles smaller than 900 μm, frequently displaying hematite replacement (martitization) along edges and cleavage lines. Magnetite also occurs as mixed particles with hematite, ilmenite, or gangue minerals, forming reticular and veined intergrowths, with ilmenite-magnetite composite edges (Figure 7A). Ilmenite (25%) occurs as free particles up to 800 μm in size, with some mixed ilmenite-magnetite grains but without evidence of replacement (Figure 7A). Hematite (15%) is primarily a replacement product of magnetite, occurring as free particles smaller than 1,000 μm or as mixed hematite-limonite (Fe<sub>2</sub>O<sub>3</sub> · FeO(OH) · nH<sub>2</sub>O) and magnetite-hematite, displaying replacement textures such as reticulate, graphitic, semi-crowned, or veined geometries. Gangue minerals (Figure 7B) account for approximately 10% quartz (SiO<sub>2</sub>), 4% rutile

(TiO<sub>2</sub>), 4% zircon (ZrO<sub>2</sub>), 2% andalusite (Al<sub>2</sub>SiO<sub>5</sub>), and 2% clays (Al<sub>2</sub>O<sub>3</sub> · 2SiO<sub>2</sub> · 2H<sub>2</sub>O). Trace minerals (<1%) include muscovite (KAl<sub>2</sub>(AlSi<sub>3</sub>O<sub>10</sub>)(OH)<sub>2</sub>), limonite (FeO(OH)·nH<sub>2</sub>O), and pyrite (FeS<sub>2</sub>). Quartz (SiO<sub>2</sub>) is the most abundant gangue mineral, occurring as free particles smaller than 900 μm, with anhedral forms, and as mixed particles associated with clays (Figure 7C). Rutile (TiO<sub>2</sub>) is present as free particles up to 400 μm and as mixed earthy textures with quartz and clays (Figure 7C). Zircon (ZrO<sub>2</sub>) appears as tabular, prismatic, or rounded euhedral particles smaller than 350 μm, usually as free grains (Figures 7C and 7D). Andalusite (Al<sub>2</sub>SiO<sub>5</sub>) occurs as free anhedral particles smaller than 500 μm, while clays (Al<sub>2</sub>O<sub>3</sub> · 2SiO<sub>2</sub> · 2H<sub>2</sub>O) form aggregates associated with quartz, rutile, or opaque mineral inclusions. Muscovite (KAl<sub>2</sub>(AlSi<sub>3</sub>O<sub>10</sub>)(OH)<sub>2</sub>) is observed as rare anhedral crystals smaller than 100 μm, exhibiting feathery structures associated with quartz. Limonite (FeO(OH)·nH<sub>2</sub>O) is found as free or mixed particles with hematite and magnetite. Pyrite (FeS<sub>2</sub>) appears sporadically as free particles ranging from 70 μm to 1,000 μm, with some containing hematite inclusions. Native gold (Au) occurs in trace amounts as free particles smaller than 400 μm, occasionally associated with gangue minerals. A total of 33 native gold particles were identified in the DAI-02 sample, with 82% measuring above 106 μm (primarily larger than 300 μm) and 18% ranging between 33 and 75 μm (Table 2). Free gold particles are commonly associated with magnetite and hematite, with minor associations with ilmenite, goethite, and gangue minerals (Figures 7A and 8B).

### ***CQI-04 sample***

The CQI-04 sample consists primarily of free particles of ilmenite (FeTiO<sub>3</sub>) and hematite (Fe<sub>2</sub>O<sub>3</sub>), with minor gangue minerals. Magnetite (Fe<sub>3</sub>O<sub>4</sub>) and rutile (TiO<sub>2</sub>) occur in trace amounts. Ilmenite particles (FeTiO<sub>3</sub>) are generally smaller than 300 μm, occasionally mixed with hematite and rutile. Hematite (Fe<sub>2</sub>O<sub>3</sub>) appears as free particles smaller than 250 μm, while gangue minerals are typically smaller than 400 μm. Free ilmenite and hematite particles exhibit subangular to rounded shapes. In the CQI-04 sample, 22 native gold particles were identified, all measuring above 106 μm (Table 2). Free gold is primarily associated with ilmenite and gangue minerals, with minor associations with hematite and magnetite (Figures 7C and 8D) (Table 3).

### **Scanning Electron Microscopy**

The Scanning Electron Microscopy study was conducted on samples DAI-02 and DAI-Hg-06 from the Puerto Belén concession, and sample CQI-04 from the Raúl 1 concession.

### ***DAI-02 sample***

The minerals identified in the DAI-02 sample include iron oxides such as magnetite ( $\text{Fe}_3\text{O}_4$ ) and hematite ( $\text{Fe}_2\text{O}_3$ ); iron and titanium oxides like ilmenite ( $\text{FeTiO}_3$ ) and ulvöspinel ( $\text{TiFe}_2\text{O}_4$ ); iron hydroxides such as goethite ( $\alpha\text{-Fe}^{3+}\text{O}(\text{OH})$ ); iron sulfides including sphalerite ( $\text{ZnS}$ ), galena ( $\text{PbS}$ ), pyrite ( $\text{FeS}_2$ ), and pyrrhotite ( $\text{Fe}_{(1-x)}\text{S}$ ); tin oxides like cassiterite ( $\text{SnO}_2$ ); sulfates such as barite ( $\text{BaSO}_4$ ); tungsten-iron oxides like ferberite ( $\text{Fe}^{2+}\text{WO}_4$ ); native gold ( $\text{Au}$ ); and rare earth minerals, including phosphates such as cerium monazite ( $(\text{Ce},\text{La})\text{PO}_4$ ), neodymium monazite ( $(\text{Nd},\text{Ce},\text{La})\text{PO}_4$ ), and xenotime ( $\text{YPO}_4$ ); yttrium silicates ( $\text{Y}_2\text{SiO}_5$ ); thorium oxides such as thorianite ( $\text{ThO}_2$ ); nesosilicates like thorite ( $(\text{Th},\text{U})\text{SiO}_4$ ); and zircon ( $\text{ZrO}_2$ ). Gold particles in the DAI-02 sample range from 50  $\mu\text{m}$  to 400  $\mu\text{m}$  in size, exhibiting elongated morphology and rounded edges (Figures 8A and 9B). Hematite ( $\text{Fe}_2\text{O}_3$ ) particles range from 50  $\mu\text{m}$  to 500  $\mu\text{m}$ , with rounded shapes and subangular edges. Magnetite ( $\text{Fe}_3\text{O}_4$ ) and ilmenite ( $\text{FeTiO}_3$ ) particles vary from 30  $\mu\text{m}$  to 500  $\mu\text{m}$ , with elongated morphology and subangular to subrounded edges. Goethite ( $\alpha\text{-Fe}^{3+}\text{O}(\text{OH})$ ) particles measure between 5  $\mu\text{m}$  and 300  $\mu\text{m}$ , with under-rounded edges. Cassiterite ( $\text{SnO}_2$ ) particles range from 100  $\mu\text{m}$  to 600  $\mu\text{m}$ , exhibiting elongated and rounded morphologies with subangular edges. Sulfide minerals such as galena ( $\text{PbS}$ ) and pyrrhotite ( $\text{Fe}_{(1-x)}\text{S}$ ) range from 5  $\mu\text{m}$  to 200  $\mu\text{m}$ , with subrounded to angular morphology. Phosphates such as monazite ( $(\text{Ce},\text{La})\text{PO}_4$ ) and xenotime ( $\text{YPO}_4$ ) range from 5  $\mu\text{m}$  to 100  $\mu\text{m}$ , with elongated morphology and subrounded edges.

### ***DAI-Hg-06 sample***

The DAI-Hg-06 sample contains native gold ( $\text{Au}$ ); quartz ( $\text{SiO}_2$ ); iron oxides such as magnetite ( $\text{Fe}_3\text{O}_4$ ) and hematite ( $\text{Fe}_2\text{O}_3$ ); iron and titanium oxides like ilmenite ( $\text{FeTiO}_3$ ), titanomagnetite ( $\text{Fe}^{2+}(\text{Fe}^{3+},\text{Ti})_2\text{O}_4$ ), and ulvöspinel ( $\text{TiFe}_2\text{O}_4$ ); tin oxides such as cassiterite ( $\text{SnO}_2$ ); zircon ( $\text{ZrO}_2$ ); aluminum silicates ( $\text{SiFeAl}$ ); and REE minerals including neodymium monazite ( $(\text{Nd},\text{Ce},\text{La})\text{PO}_4$ ) and xenotime ( $\text{YPO}_4$ ); as well as niobium oxides such as fergusonite ( $(\text{Ce},\text{Nd},\text{Y})\text{NbO}_4 \cdot 0.3\text{H}_2\text{O}$ ). Gold particles in the DAI-Hg-06 sample range from 25  $\mu\text{m}$  to 400  $\mu\text{m}$ , with elongated morphology and under-rounded edges (Figures 8E and 9F). Magnetite ( $\text{Fe}_3\text{O}_4$ ) particles measure between 150  $\mu\text{m}$  and 320  $\mu\text{m}$ . Ilmenite

(FeTiO<sub>3</sub>) particles range from 100 µm to 400 µm, with elongated morphology and rounded to subangular edges. Hematite (Fe<sub>2</sub>O<sub>3</sub>) particles measure between 100 µm and 150 µm, with subrounded morphology and subangular edges.

### ***CQI-04 sample***

The CQI-04 sample contains native gold (Au); quartz (SiO<sub>2</sub>); iron and titanium oxides such as ilmenite (FeTiO<sub>3</sub>) and ulvöspinel (TiFe<sub>2</sub>O<sub>4</sub>); zircon (ZrO<sub>2</sub>); and REE minerals, including monazite ((Ce,La,Nd)PO<sub>4</sub>). Gold particles range from 50 µm to 1,250 µm, exhibiting elongated and under-rounded morphology with subrounded to subangular edges (Figures 9C and 9D). Zircon (ZrO<sub>2</sub>) particles range from 500 µm to 950 µm, with elongated morphology and under-rounded edges (Figure 8). Quartz (SiO<sub>2</sub>) particles measure between 700 µm and 800 µm, with subrounded morphology and subangular to subrounded edges. Ilmenite (FeTiO<sub>3</sub>) grains measure 900 µm in size, with subrounded morphology and subangular edges. Ulvöspinel (TiFe<sub>2</sub>O<sub>4</sub>) grains are 600 µm in size, with elongated morphology and rounded edges. Monazite ((Ce,La)PO<sub>4</sub>) particles range from 600 µm to 900 µm, with subrounded morphology and subangular edges.

### ***Gold Purity Analysis***

The six spectra analyzed from the DAI-02 sample indicate an average Au content of 99.09% and Ag of 0.92%. The twelve spectra analyzed from the DAI-Hg-06 sample show an average Au content of 99.02% and Ag of 0.98%. The nine spectra analyzed from the CQI-04 sample show an average Au content of 99.00% and Ag of 1.04%, confirming the high purity of native gold in all samples. The CQI-04 sample exhibited a greater number of gold particles and larger particle sizes compared to the DAI-02 and DAI-Hg-06 samples (Table 3).

### ***Valued mesh***

Samples DAI-01 and CQI-05, belonging to the Puerto Belén concession and Raul 1 concession, respectively, were sieved by meshes 60, 100, 150, 200, and 325. The distribution of gold in the sample DAI-01, indicates that 80.98% of free gold particles are concentrated on mesh 60 (+m60), 2.40% is below mesh 60 and above mesh 100 (-m60 and +m100), 1.60% is below mesh 100 and above mesh 150 (-m100

and +m150), 2.14% is below mesh 150 and above mesh 200 (-m150 and +m200), 5.01% is below 200 mesh and above 325 mesh (-m200 and +m325), and 7.87% is below 325 mesh (-m325) (Figure 10). The distribution of gold in the CQI-05 sample indicates that the 23.12% of free gold particles are concentrated on mesh 60 (+m60), 31.19% is below mesh 60 and above mesh 100 (-m60 and +m100), 18.14% is below 100 mesh and above 150 mesh (-m100 and +m150), 13.36% is below 150 mesh and above 200 mesh (-m150 and +m200), 5.07% is below 200 mesh and above 325 mesh (-m200 and +m325), and 9.12% is below 325 mesh (-m325).

## DISCUSSION

### Possible Relationships Between Mineral Content, Particle Size, and Economic Elements

The results show a clear relationship between mineralogical composition, gold particle size, and its stability in alluvial deposits. In the Puerto Belén concession, the high concentration of heavy minerals such as ilmenite, magnetite, and hematite coincide with the predominance of coarse gold particles (80.98%). This suggests a transition from initial high-energy transport (required to concentrate heavy minerals) to lower-energy depositional conditions, promoting gold particle stability. Such hydraulic energy decline is characteristic of mature alluvial systems (British Geological Survey, 1997), where dense minerals (e.g., ilmenite, magnetite) and coarse gold preferentially settle as flow competence drops (Youngson & Craw, 1999).

In contrast, the Raúl 1 concession presents a mineralogical composition dominated by silica and a lower proportion of heavy minerals, reflected in a more balanced gold particle size distribution: coarse (23.12%), medium (49.33%), and fine (27.55%). The higher proportion of finer particles suggests that this environment has been subjected to greater hydraulic energy, facilitating sedimentary reworking and redistributing gold into different size fractions (Alves et al., 2020). This variability may be influenced by the river dynamics in the area, which not only transport finer particles but also contribute to the differential concentration of gold depending on changes in flow velocity and sediment load.

Moreover, the presence of heavy minerals in gold-bearing deposits can impact the efficiency of gold recovery methods. High-density minerals such as magnetite and ilmenite can serve as indicators of gold

enrichment zones, as they tend to accumulate alongside gold in natural sedimentary traps. This highlights the importance of mineralogical characterization not only for assessing gold potential but also for designing optimized processing strategies for each type of deposit.

### **Gold and Other Economic Minerals Compared to Other Deposits**

The gold values obtained in the studied concessions show both similarities and differences with other alluvial deposits in the Amazonian region. In the deposits of the Madre de Dios River basin, gold purity ranges from 85% to 97% due to the presence of alloying metals such as silver, copper, and iron (Craw & Lilly, 2016). In this study, gold purity is higher (99% Au and 1% Ag), suggesting that these placer deposits have undergone a longer sedimentary maturation, allowing for the progressive removal of impurities during transport and deposition processes.

This high purity not only represents an economic advantage but also suggests that the gold in these concessions has been less exposed to heavy metal contamination, as demonstrated in mature Amazonian placers (Palacios-Torres et al., 2020). The low concentration of trace elements could be related to specific geochemical conditions at the primary source. In particular, the original gold mineralization may have originated from orogenic deposits and low-sulfidation hydrothermal systems, given the low content of silver, copper, and lead. Additionally, the presence of accessory minerals such as zircon, monazite, and rutile suggest a possible association with granitic intrusions and pegmatites, which may have influenced the formation and subsequent release of gold into the sedimentary environment.

In southern Peru, accessory minerals such as zircon, monazite, and rutile have been identified in alluvial deposits and placers in two main regions. However, their commercial exploitation due to their REE and titanium content has been limited compared to other areas of the world where these minerals are extracted on an industrial scale. In the places of the Madre de Dios, Malinowski, Lower Inambari, and Tambopata rivers, the presence of tin, ilmenite, rutile, zircon, and monazite has been recorded, with yellow monazite reaching a maximum grade of 1.2% in the concentrates from the Malinowski River (Lanckneus, 1991). Likewise, in the placers of the Vilcanota River in Cusco, commercially interesting heavy minerals such as ilmenite, zircon, garnet, rutile, and monazite have been identified. However, the exploitation of these minerals in this area has not been widely documented or developed on a large scale (Delgado & Benavente, 2011).

## **The Mercury Problem and Alternative Methods in Mineral Processing**

The use of mercury in alluvial mining remains one of the main environmental concerns in the region. It is estimated that over 180 tons of this metal are released annually into the aquatic ecosystems of the Madre de Dios River basin, causing long-term toxic impacts on both the environment and local communities. Mercury not only contaminates water and sediments but also bioaccumulates throughout the food chain, posing a significant risk to human health due to chronic exposure and the consumption of contaminated fish (AGC, 2017).

To mitigate or eliminate the use of mercury in artisanal and small-scale mining in the Madre de Dios region, the implementation of clean and environmentally sustainable technologies is proposed as a replacement for amalgamation. In the Puerto Belén concession, the high concentration of free gold particles of medium to coarse size, associated with heavy minerals such as ilmenite and magnetite, suggest that gravity-based methods such as shaking tables, spiral concentrators, and centrifugal concentrators could be efficiently employed for gold recovery. Subsequently, these concentrates could be processed using complementary techniques such as carbon and oil agglomeration (COA) or flotation to enhance gold recovery.

In the Raúl 1 concession, where gold is found in a broader granulometric distribution (fine, medium, and coarse) and is associated with a high silica content and a low proportion of iron oxides, the use of similar gravity-based methods is recommended, combined with sintering to improve gold recovery efficiency. Additionally, techniques such as COA and flotation could optimize mineral beneficiation, minimizing environmental impact and reducing dependence on mercury in alluvial gold processing.

The findings of this study not only enhance the understanding of the relationship between mineral content and gold distribution but also provide valuable insights for optimizing mineral beneficiation practices. The transition to gravity-based methods and the potential exploitation of accessory minerals represents opportunities to reduce environmental impact and diversify production in alluvial mining.

## **CONCLUSIONS**

The mineralogical characterization of the alluvial sand preconcentrates from the Puerto Belén and Raul 1 mining concessions reveals significant compositional differences with implications for economic exploitation. The Puerto Belén concession is enriched in titanium and iron oxides, primarily ilmenite (15%) and magnetite (50%). Additionally, heavy minerals such as monazite, xenotime, fergusonite, yttrium silicates, thorianite, and thorite were identified, along with REE, as well as thorium, which may represent additional economic opportunities. In contrast, the Raul 1 concession contains a significant concentration of zircon (11%). Monazite, although present in smaller quantities (<1%), represents an important REE ore. Gold particle size distribution differs between the two concessions. In Puerto Belén, over 80% of the gold is coarse-grained (greater than 250  $\mu\text{m}$ ), primarily in the form of gold leaves and nuggets. In Raul 1, gold particles are more evenly distributed, with 50% classified as medium-sized (106–250  $\mu\text{m}$ ), 28% as fine (<106  $\mu\text{m}$ ), and 23% as coarse (>250  $\mu\text{m}$ ). In both concessions, the native gold exhibits high purity, with an average composition of 99% Au and 1% Ag. The mineralogical composition and gold particle size analysis have provided valuable insights into the spatial distribution of economic minerals and highlight the potential for further exploration of iron, titanium, zirconium, thorium, and REE in the region.

## Acknowledgments

Thanks to BIZAlab S.A.C., Metalurgia Silver S.A.C (METASIL) and Athena Minerals geologist team. This research has been partially funded by the Artisanal Gold Council.

## REFERENCES

- Alves, K.D.S., Sánchez, S.B., Barreiro, J.G., Palomares, R.M., & Prieto, J.M.C. (2020). *Morphological and compositional analysis of alluvial gold: The Fresnedoso gold placer (Spain)* [Journal article]. *Ore Geology Reviews*, 121, 103489. <https://doi.org/10.1016/j.oregeorev.2020.103489>
- Artisanal Gold Council (AGC). (2017). *Estimaciones de referencia del uso y consumo de mercurio en la minería de oro artesanal y de pequeña escala en Perú* [Proyecto: Plan Nacional de Acción sobre Mercurio en el sector de la Minería de oro Artesanal y de Pequeña escala en el Perú].
- Artisanal Gold Council (AGC). (2022). *Reporte interno: Piloto IV uso de tecnologías limpias libre de mercurio*.



- Aranda, A. (1999). Hacia la localización de minerales pesados en el Perú. *Simposium Internacional de Minerales Industriales del Perú*, Lima, INGEMMET, Minerales industriales del Perú, p. 249-253.
- Azañero, A. (1998). Oro aluvial: Alternativas de beneficio metalúrgico. *Revista del Instituto de Investigación de la Facultad de Minas, Metalurgia y Ciencias Geográficas*, 1(1), 31-41. <https://doi.org/10.15381/iigeo.v1i1.2303>
- British Geological Survey, Mineralogical and Petrologic Group. (1997). *A review of gold particle-size and recovery methods* [Technical report WC/97/14]. C.J. Mitchell, E.J. Evans y M.T. Styles.
- Campbell, K. E., & Romero, L. (1989). La geología del Cuaternario del Departamento de Madre de Dios. *Boletín de la Sociedad Geológica del Perú*, 79, 53-61.
- Craw, D., & Lilly, K. (2016). *Gold nugget morphology and geochemical environments of nugget formation, southern New Zealand* [Journal article]. *Ore Geology Reviews*, 79, 301-315. <https://doi.org/10.1016/j.oregeorev.2016.06.001>
- Delgado, J. (2019). Relación entre la amalgamación con mercurio para recuperar oro y el grado de contaminación del suelo [Master's thesis]. Universidad Nacional de San Agustín de Arequipa.
- Delgado Madera, G. F., & Benavente Escobar, C. L. (2011). *Evaluación del río Vilcanota en el distrito de San Salvador, provincia de Calca - región Cusco*.
- Guyot, J. L., Jouanneau, J. M., Soares, L., Boaventura, G. R., Maillet, N., & Lagane, C. (2007). Clay mineral composition of river sediments in the Amazon Basin. *CATENA*, 71(2), 340-356. <https://doi.org/10.1016/J.CATENA.2007.02.002>
- Huamán, F., Palma, G., & Flores, L. (2020). Caracterización preliminar de residuos de minería aluvial en la región Madre de Dios – Perú. *Revista Cubana de Química*, 32(2), 232-244. [http://scielo.sld.cu/scielo.php?script=sci\\_arttext&pid=S222454212020000200232](http://scielo.sld.cu/scielo.php?script=sci_arttext&pid=S222454212020000200232).
- Instituto de Investigaciones de la Amazonía Peruana (IIAP) & Ministerio del Ambiente (MINAM). (2011). *Minería aurífera en Madre de Dios y contaminación con mercurio*.
- Instituto Geológico, Minero y Metalúrgico (INGEMMET). (2003). *Reconocimiento de las actividades mineras y metalúrgicas en la cuenca de los ríos Madre de Dios e Inambari*.
- Lanckneus, J. (1991). Los placeres auríferos de Madre de Dios (SE Perú). *Alluvial Gold Placers*, G. Herai & M. Fornari (eds.). Actes du Symposium Intern, sur les gisements alluviaux d'or. La Paz, 3-5 junio 1991, 89-102.
- La Riva, G. (1991). Facies fluviales identificadas en depósitos de point bar del río Madre de Dios, (Departamento de Madre de Dios, Perú).
- Ledesma, P. (2021). Caracterización de oro y minerales de tierras raras en depósitos fluviales tipo placer del río Madre de Dios [Undergraduate thesis]. Universidad Nacional de Ingeniería.
- Mathioudakis, S., Xiroudakis, G., Petrakis, E., & Manoutsoglou, E. (2023). *Alluvial gold mining technologies from ancient times to the present* [Journal article]. *Mining*, 3(4), 618-644. <https://doi.org/10.3390/mining3040034>
- Medina, G. (1999). Minerales pesados en gravas auríferas de Huepetuhe y Caychive (Madre de Dios). *Simposium Internacional de Minerales Industriales del Perú*, Lima, PE, 18-20 agosto 1999, Minerales industriales del Perú, Lima: INGEMMET, pp. 254-259.

- Mosquera, C., Chávez, M., Pachas, V., & Moschella, P. (2009). Estudio diagnóstico de la actividad minera artesanal en Madre de Dios.
- Navarro, G. (2017). Estudio de la recuperación de oro aluvial en concentrador Falcon en la Cooperativa Minera LIMATA Ananea – Puno [Undergraduate thesis]. Universidad Nacional Jorge Basadre Grohmann.
- Nikitina, D., Remizova, L., & Losco, R. (2011). A preliminary investigation of the soils and geomorphology of a portion of the Madre de Dios region, Peru. *Soil Horizons*, 52(2), 40. <https://doi.org/10.2136/sh2011.2.0040>
- Osores, F., Rojas, J., Manrique, C. (2012). Minería informal e ilegal y contaminación con mercurio en Madre de Dios: Un problema de salud pública. *Acta médica peruana*, 29(1), 1–5.
- Palacios, O., Molina, O., Galloso, A., & Reyna, C. (1996). Geología de los cuadrángulos de Puerto Luz, Colorado, Laberinto, Puerto Maldonado, Quincemil, Masuco, Astillero y Reserva Tambopata. Hojas: 26-u, 26-v, 26-x, 26-y, 27-u, 27-v, 27-x, 27-y. *INGEMMET*, 81, 189. <https://hdl.handle.net/20.500.12544/37>
- Palacios-Torres, Y., De la Rosa, J. D., & Olivero-Verbel, J. (2020). Trace elements in sediments and fish from Atrato River: An ecosystem with legal rights impacted by gold mining at the Colombian Pacific. *Environmental Pollution*, 256, 113290. <https://doi.org/10.1016/j.envpol.2019.113290>.
- Prater, L. (1957). Black Sands. *Idaho Bureau of Mines and Geology*, 1–21.
- Roddaz, M., Viers, J., Brusset, S., Baby, P., & Hérail, G. (2005). Sediment provenances and drainage evolution of the Neogene Amazonian foreland basin. *Earth and Planetary Science Letters*, 239(1–2), 57–78. <https://doi.org/10.1016/J.EPSL.2005.08.007>.
- Sousa, R. N., Veiga, M. M., Klein, B., Telmer, K., Gunson, A. J., & Bernaudat, L. (2010). Strategies for reducing the environmental impact of reprocessing mercury-contaminated tailings in the artisanal and small-scale gold mining sector: Insights from Tapajos River Basin, Brazil. *Journal of Cleaner Production*, 18(16–17), 1757–1766. <https://doi.org/10.1016/j.jclepro.2010.06.016>.
- Teixeira, R., Pereira, W., Souza, E., Ramos, S., Dias, Y., Lima, M., de Souza Neto, H., Oliveira, E., & Fernandes, A. (2021). Artisanal gold mining in the eastern Amazon: Environmental and human health risks of mercury from different mining methods. *Chemosphere*, 284, 131220. <https://doi.org/10.1016/J.CHEMOSPHERE.2021.131220>.
- Uba, C. E., Strecker, M. R., & Schmitt, A. K. (2007). Increased sediment accumulation rates and climatic forcing in the central Andes during the late Miocene. *Geology*, 35(11), 979–982. <https://doi.org/10.1130/G224025A.1>.
- USAID. (2021). *La minería ilegal en la Amazonía peruana*.
- Velásquez, M. (2017). Metales en suelos explotados por la pequeña minería aurífera aluvial en Madre de Dios, Perú [Undergraduate thesis]. Universidad Nacional Agraria la Molina.
- Villachica, C., Llamosas, J., & Villachica, L. (2010). Oro ecológico: Tecnología para la obtención de oro sin mercurio en la minería de pequeña escala.
- Youngson, J. H., & Craw, D. (1999). Variation in placer style, gold morphology, and gold particle behavior down gravel bed-load rivers: An example from the Shotover/Arrow-Kawarau-Clutha River system, Otago, New Zealand. *Economic Geology*, 94(5), 615–634. <https://doi.org/10.2113/gsecongeo.94.5.615>

FIGURES

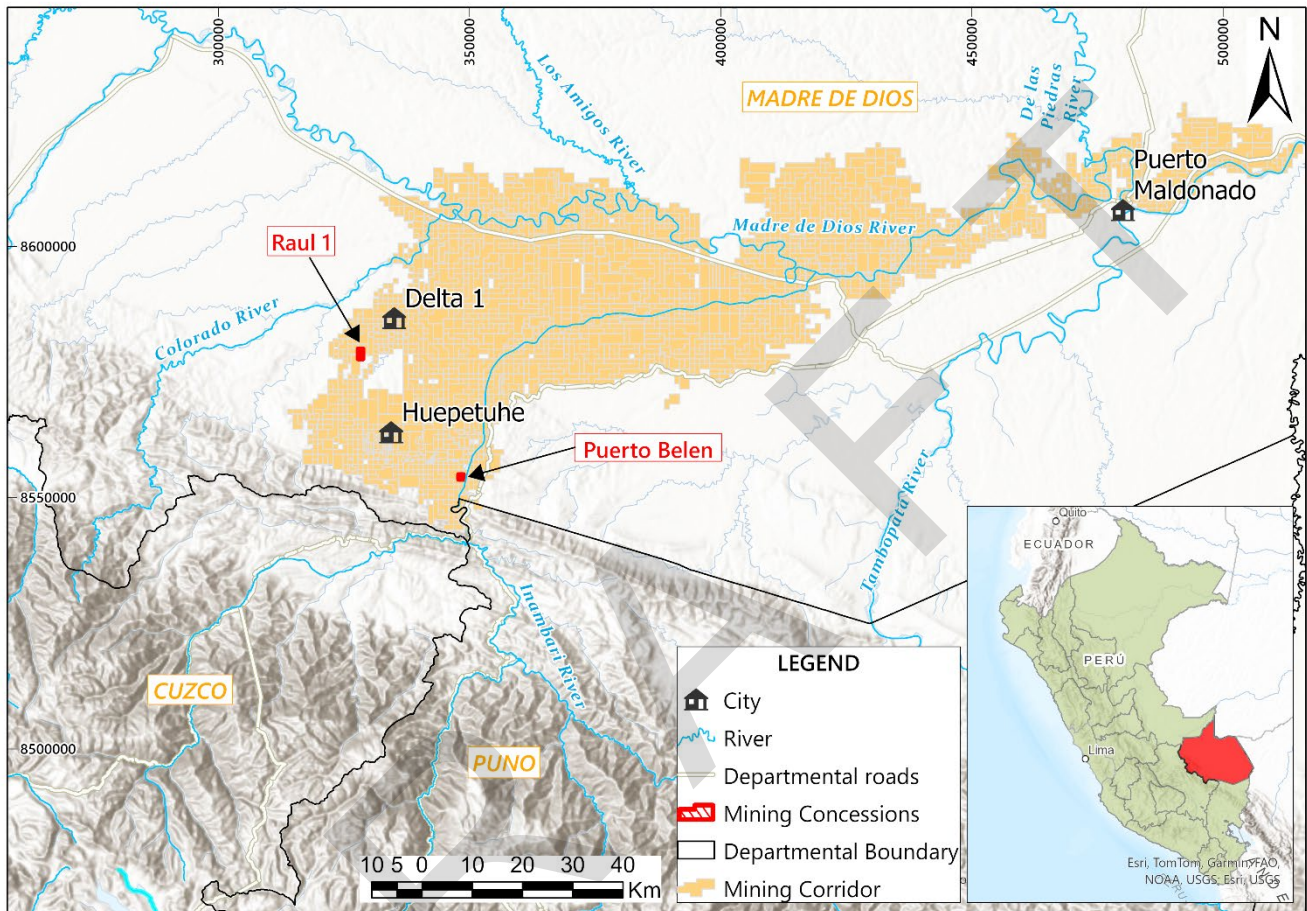


Figure 1. Map of location and accessibility to the mining concessions of Puerto Belén and Raul 1.

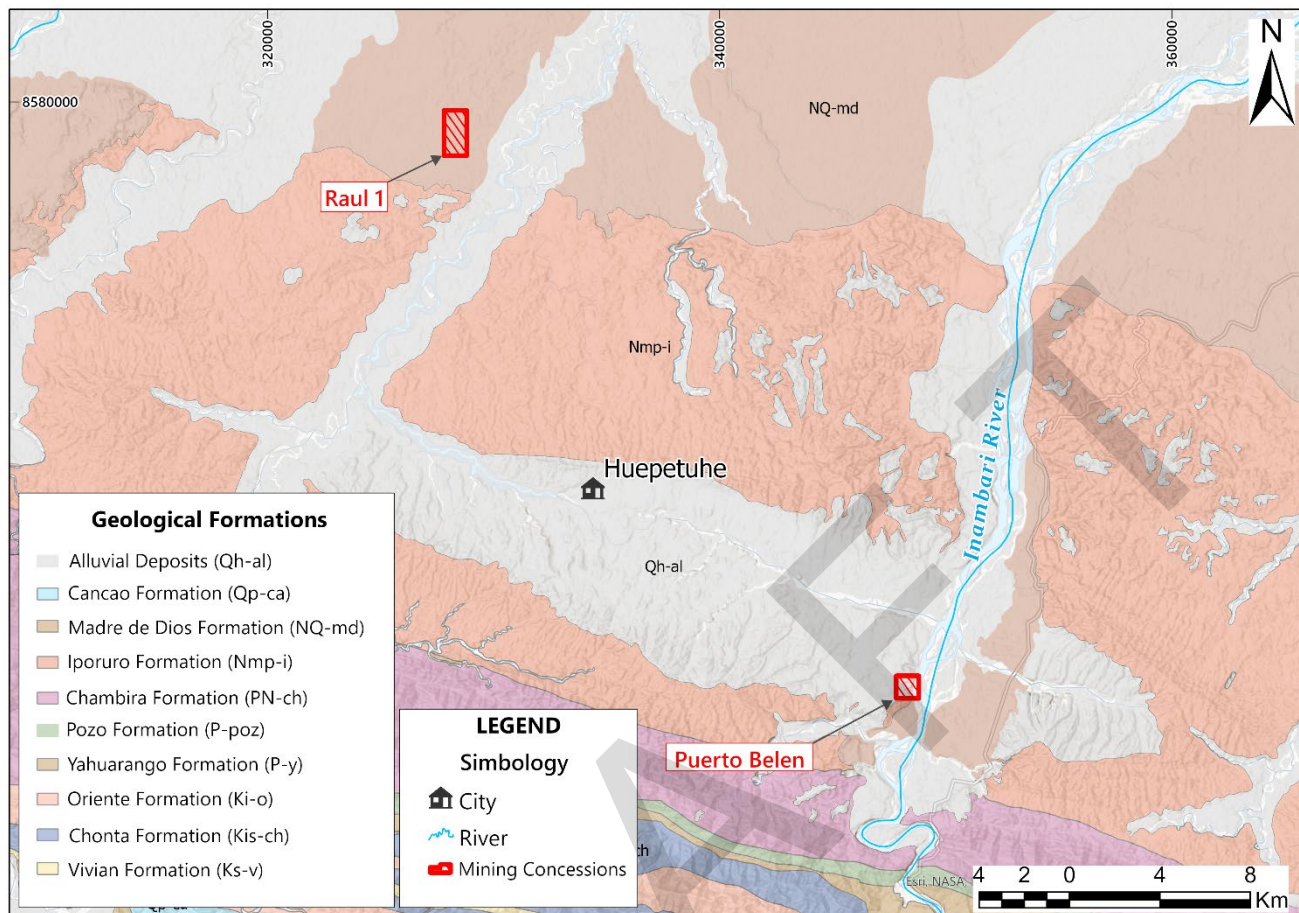


Figure 2. Geological map of the study area.

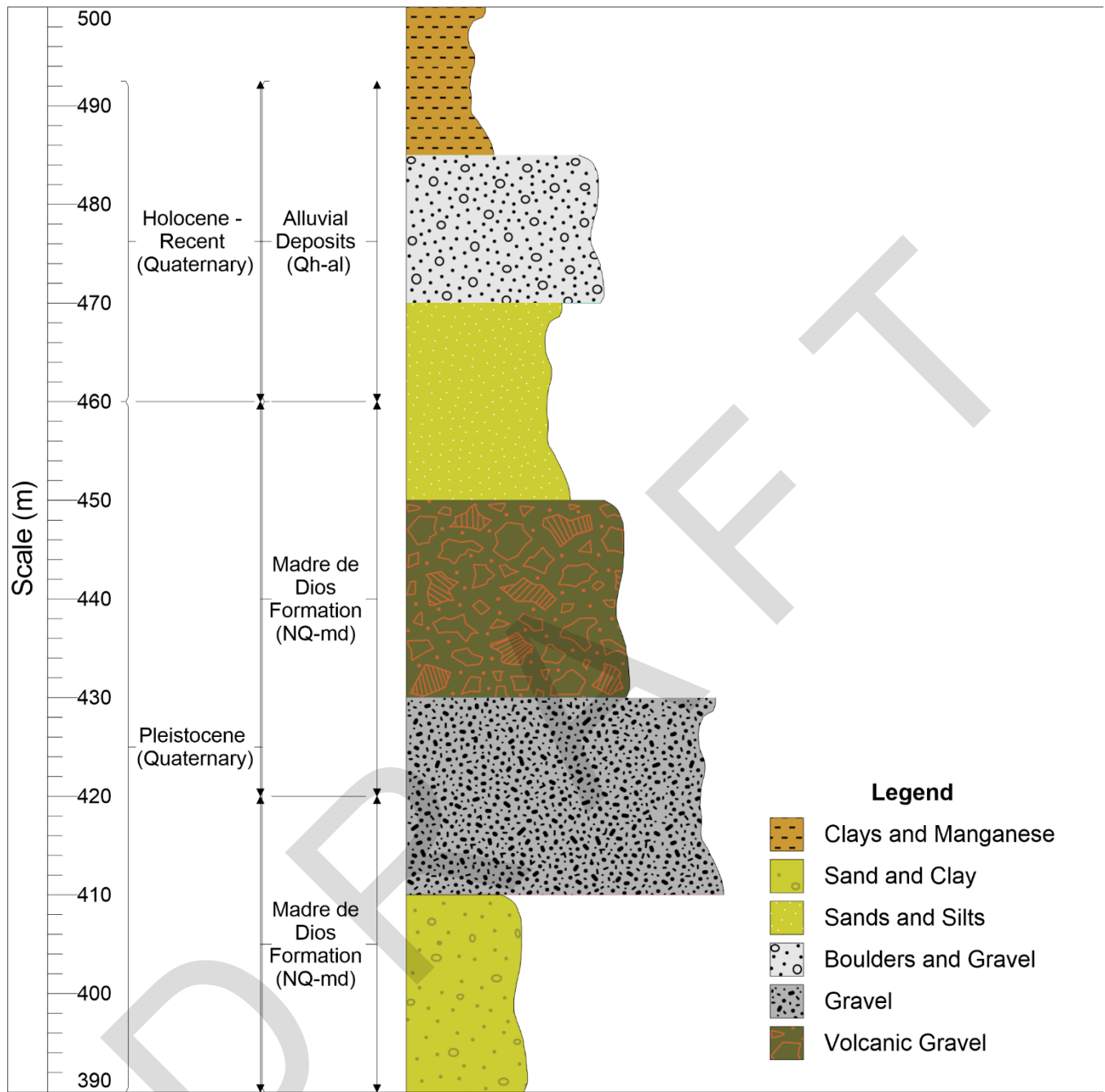


Figure 3. General stratigraphic column of Puerto Belén.

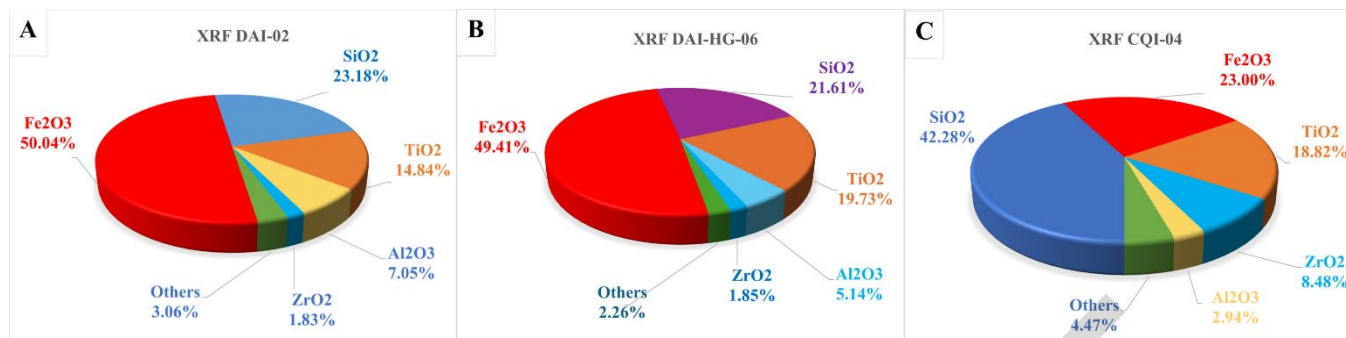


Figure 4. X-ray Fluorescence (XRF) analysis of preconcentrate samples from the Puerto Belén concession (DAI-02, DAI-Hg-06) and the Raul 1 concession (CQI-04).

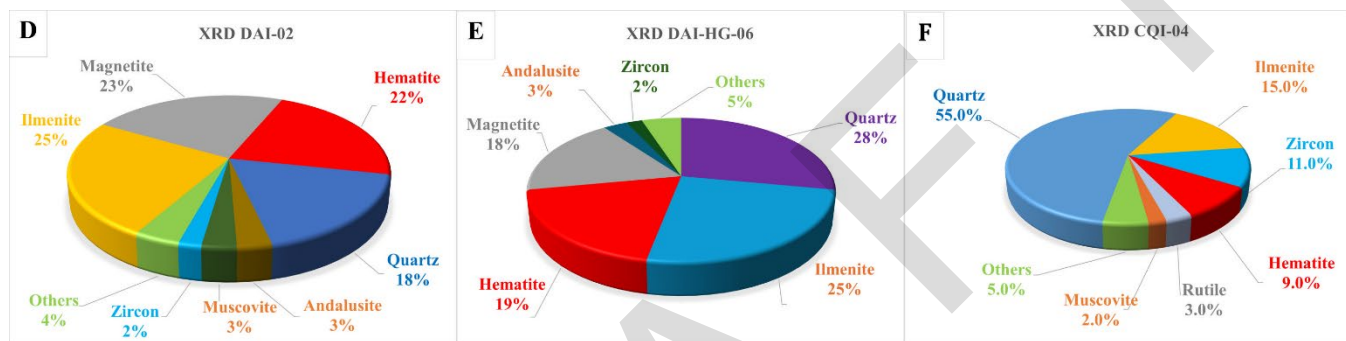


Figure 5. X-ray Diffraction (XRD) analysis of preconcentrate samples from the Puerto Belén concession (DAI-02, DAI-Hg-06) and the Raul 1 concession (CQI-04).

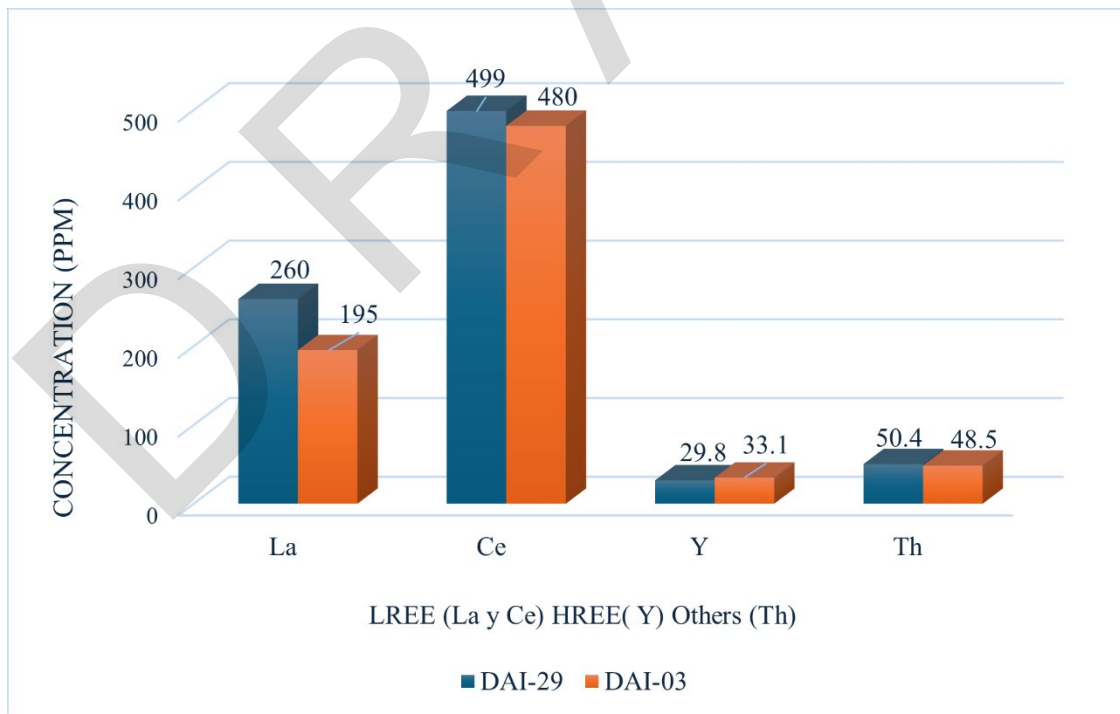


Figure. 6 Anomalies in REE and Th in the preconcentrates of the Puerto Belén concession.

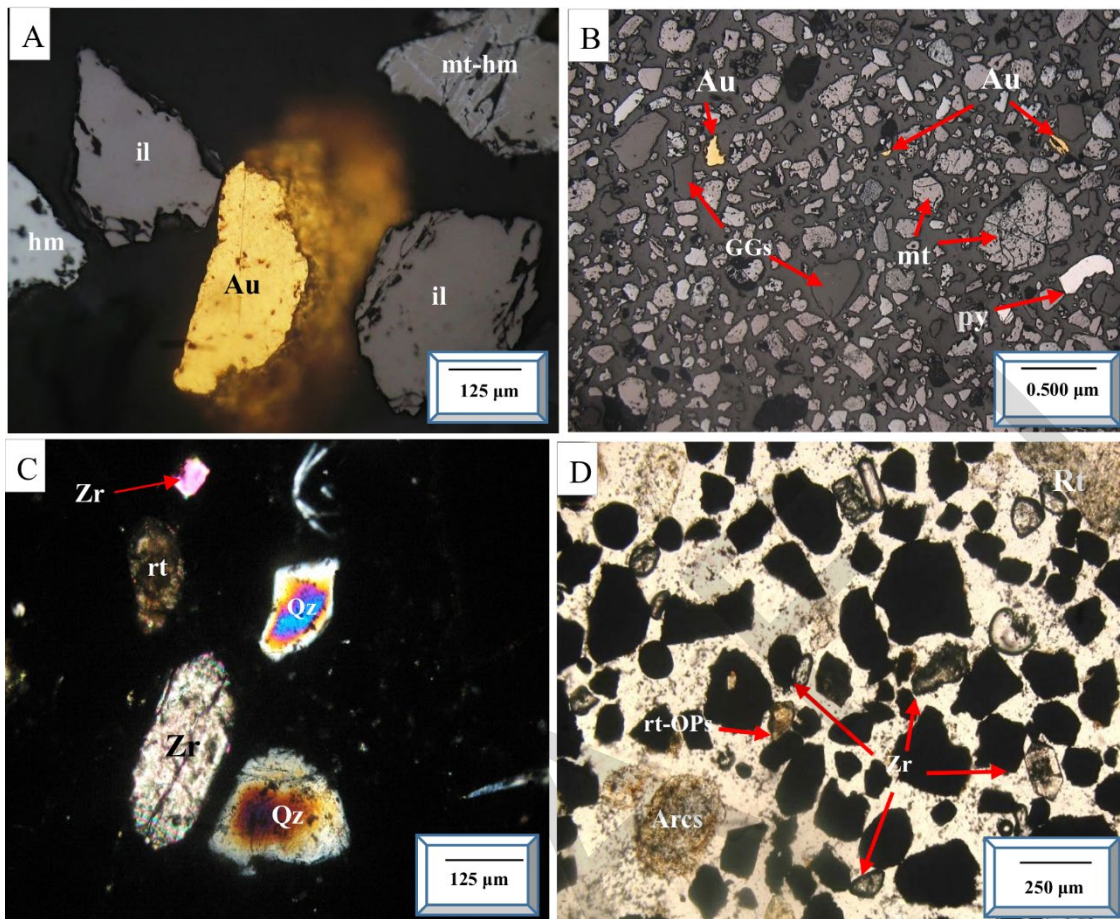


Figure. 7. Photomicrographs of light from the DAI-02 sample characteristic of the preconcentrate of the Puerto Belén concession. A. Free native gold particle and magnetite particle replaced by hematite, showing the process of martyrization. B. Free native gold particles with sizes between 160 and 40  $\mu\text{m}$ , associated with magnetite (mt), hematite (hm), ilmenite (il) and gangues (GGs). C. Anhedral and free quartz particles (Qz), very high relief zircon grain (Zr), rutile grain (rt), opaque mineral particles (OPs). D. Exposure of trace minerals showing euhedral particles of zircon (Zr), clays (ARCs), rutile (rt) and mixed grain of rutile and opaque minerals (rt-OPs).

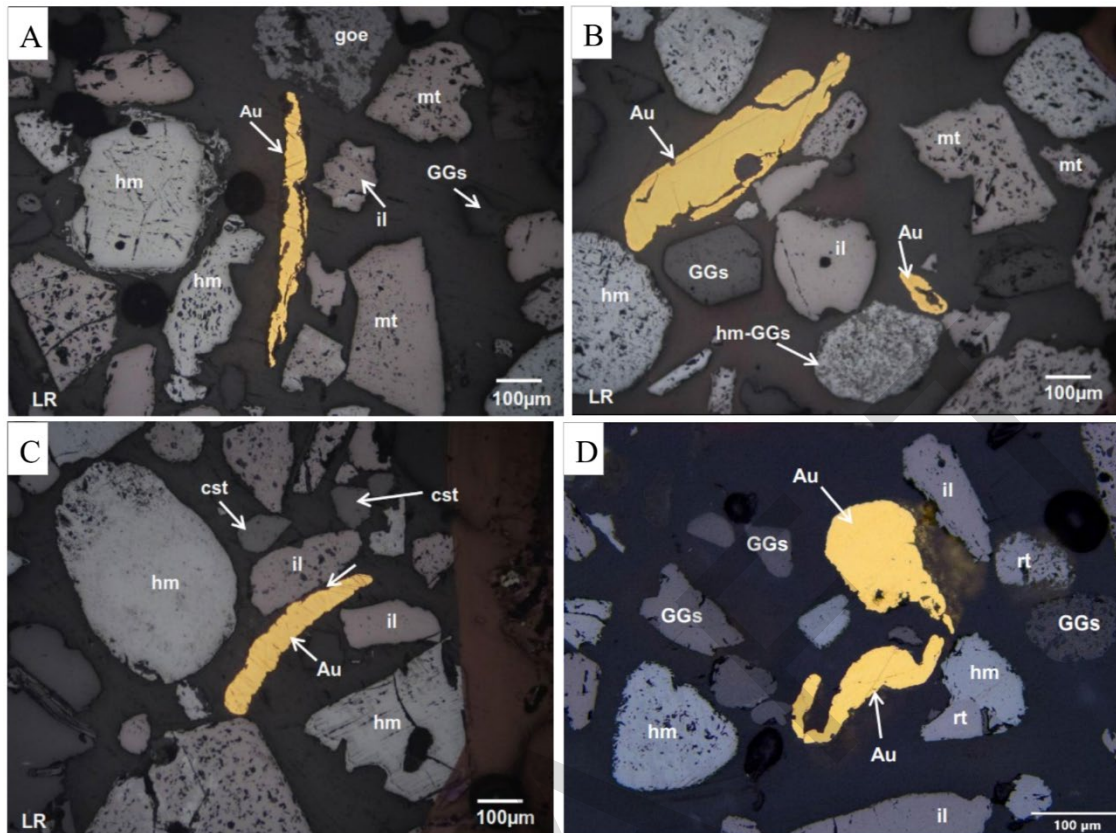


Figure. 8 Photomicrographs showing the different morphologies of free native gold and associated minerals in the Puerto Belén concession (6A, 6B) and the Raul 1 concession (6C, 6D). A, B. Free native gold particles associated with iron oxides such as magnetite (mt), hematite (hm), ilmenite (il) and gangues (GGs); C, D. Free native gold particles associated with iron oxides and trace minerals such as rutile (rt) and cassiterite (cst).



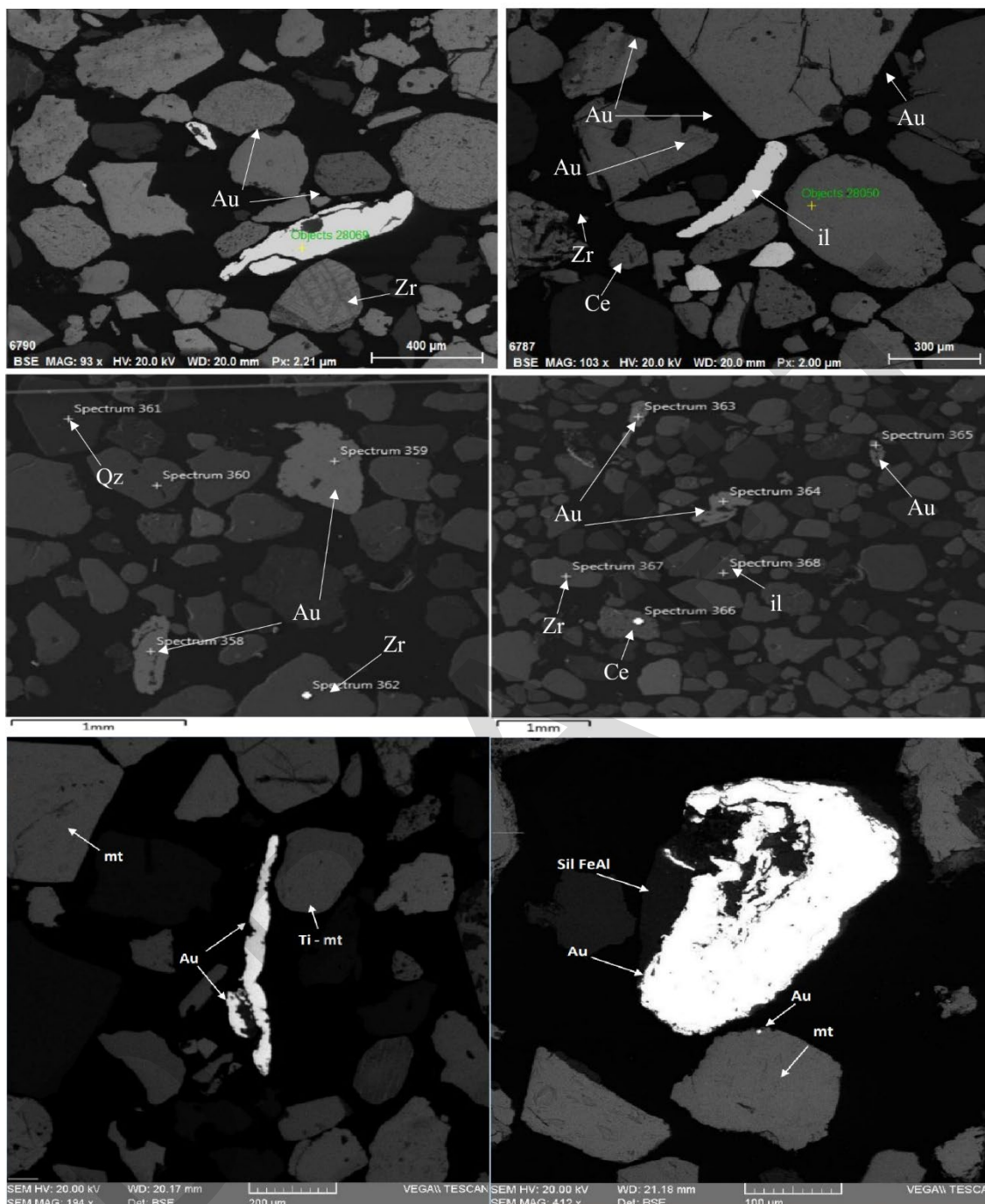


Figure. 9. Photomicrographs of three samples DAI-02, CQI-04 and DAI-Hg-06 with different morphology of free gold and associated minerals. *Sample DAI-02* (7A, 7B) A. 93x magnification shows 500  $\mu\text{m}$  free gold particles. B. Magnification of 103 x, gold particles with elongated morphology and subrounded edges of 350  $\mu\text{m}$  are appreciated. *Sample CQI-04* (7C, 7D). C. Native gold particles (Au) in spectra 358 and 359 of 800x20  $\mu\text{m}$  and 900x500 $\mu\text{m}$ , respectively. D. Native gold particles (Au) in the 363, 364 and 365 spectra of 400x100  $\mu\text{m}$ , 500x250  $\mu\text{m}$  and 400x100 $\mu\text{m}$ , respectively. *Sample DAI-Hg-06* (7E, 7F) with gold particles associated with magnetite (mt) and silicate iron and aluminum. E) Magnification of 412x, native gold particles (Au) of 300x150  $\mu\text{m}$  are appreciated. F. 194x magnification, native gold particles (Au) of 200 x 20  $\mu\text{m}$  are appreciated.

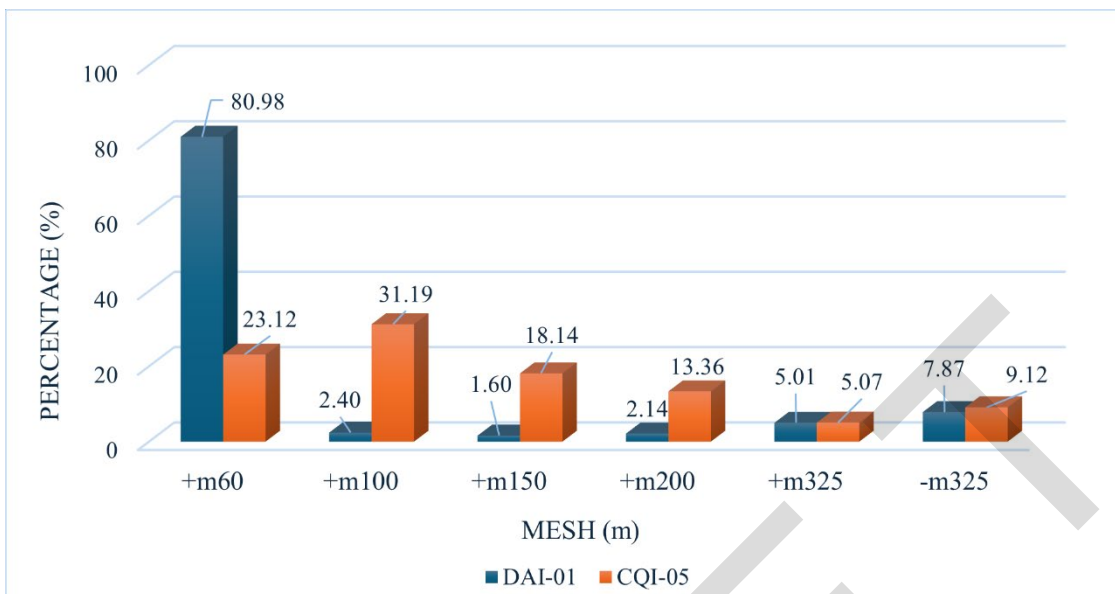


Figure. 10. Valued mesh results. Sample DAI-01 and CQI-05 - Laboratory of METASIL.

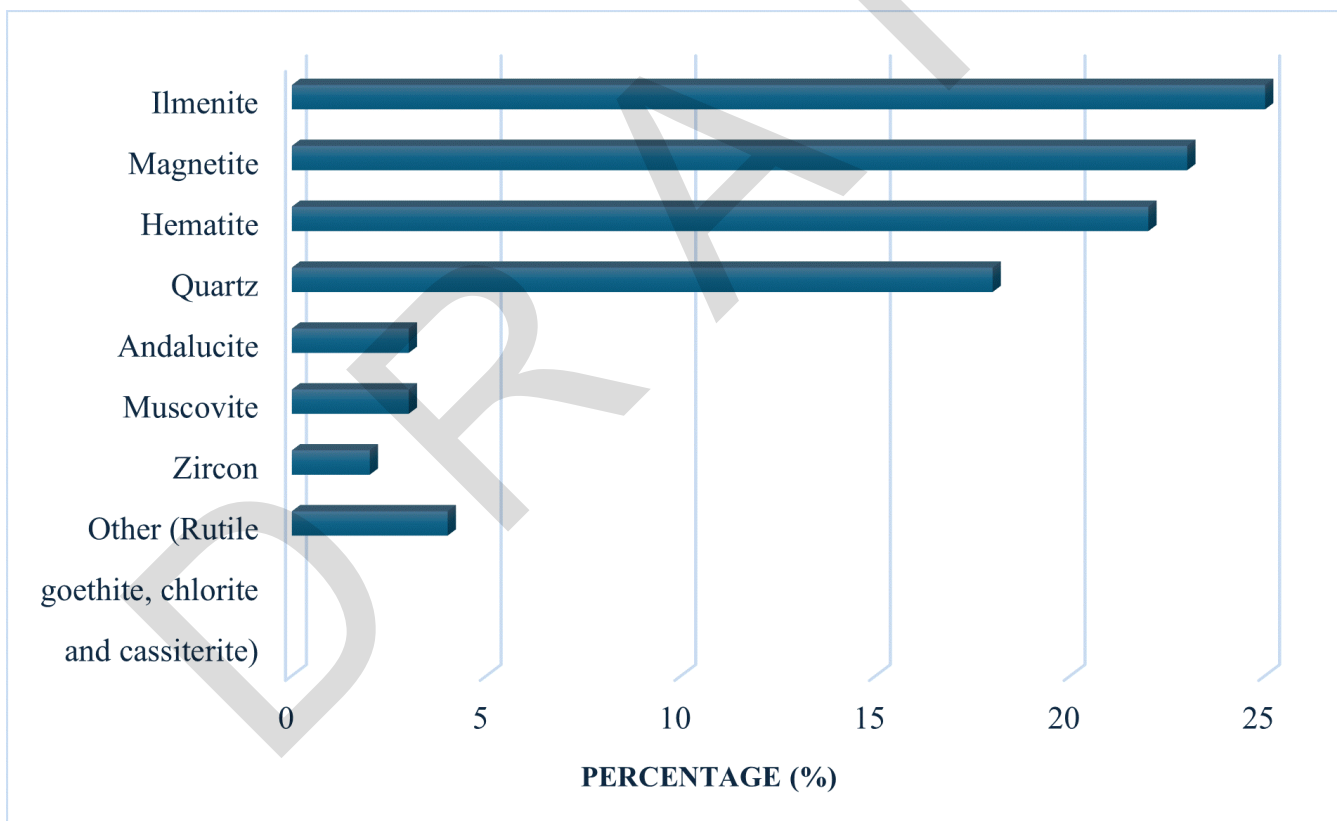


Figure. 11. DAI-02 sample analyzed by XRD.

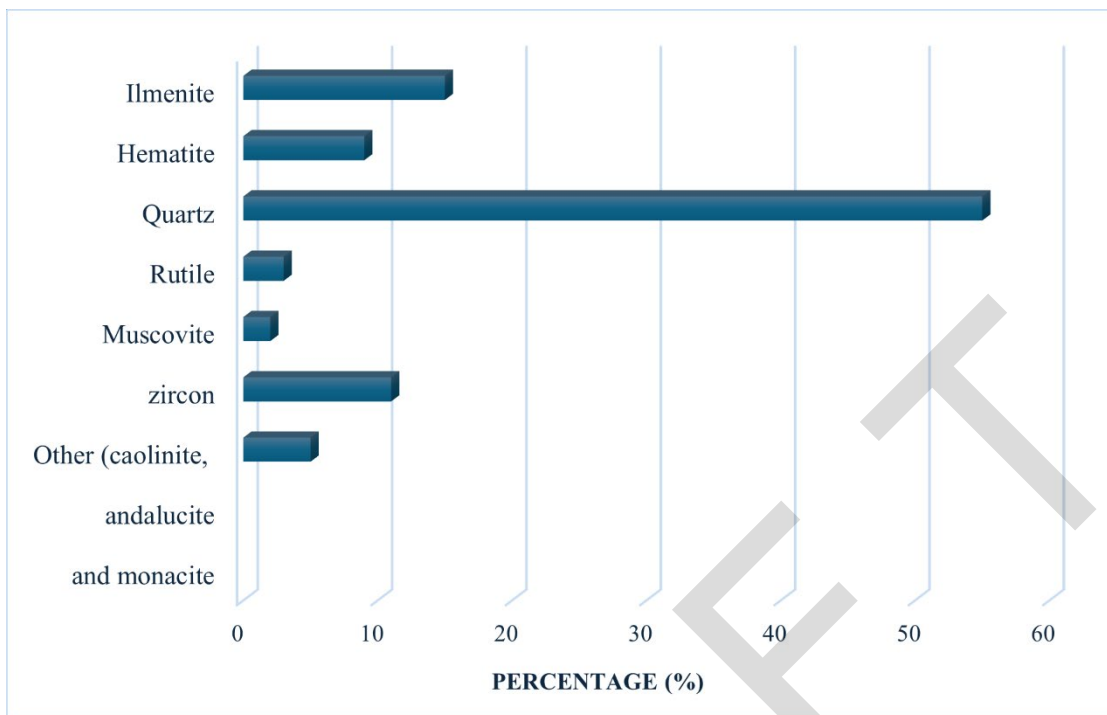


Figure 12. CQI-04 sample analyzed by XRD.

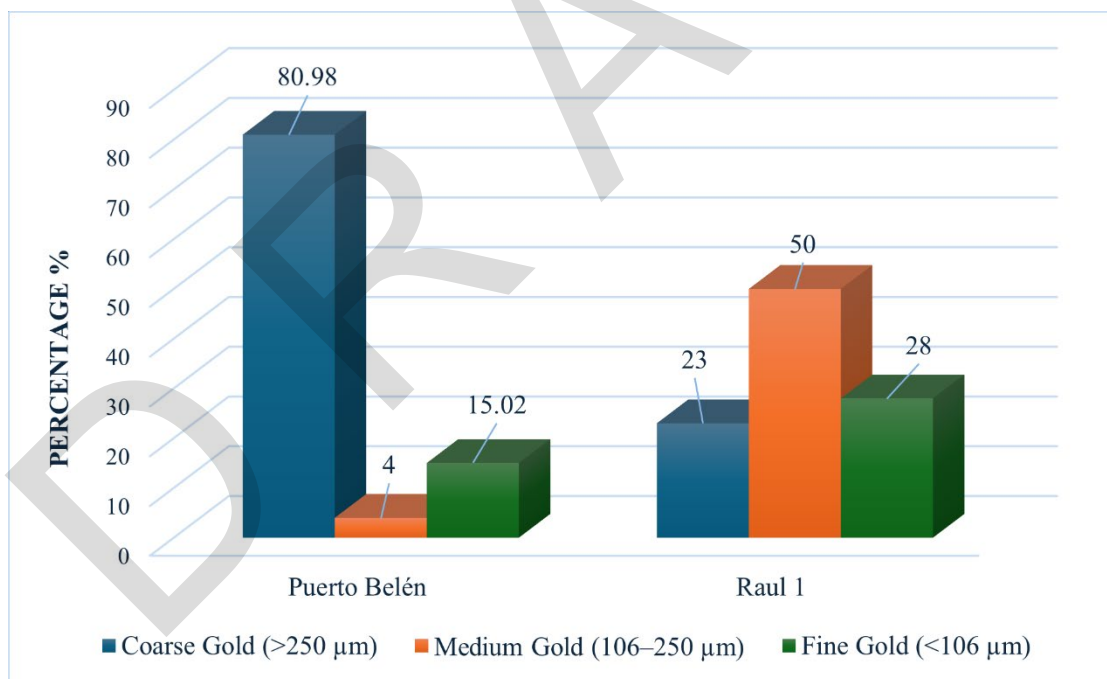


Figure 13. Size distribution of gold particles in alluvial concentrates from the Puerto Belén and Raul 1 concessions – METASIL SAC Laboratory.

**TABLES**

Table 1. Summary of our studies and other references cited.

LOCATION	CODE	SAMPLE	ESSAYS					REFERENCE
			XRD	XRF	SEM	MO*	MV**	
Delta 1 - Raul 1	CQI-04	CQI-04						This studio
		CQI-05						This studio
Huepetuhe - Puerto Belén	DAI	DAI-01						This studio
		DAI-02						This studio
		DAI-03						This studio
		DAI-29						This studio
		DAI-Hg-06						This studio
Huepetuhe	HP-01	Huepetuhe						INGEMMET (2003)
Inambari Bajo	INGEMMET	Río Inambari						INGEMMET (2003)
CH***Inambari	MF1	-						Huaman et.al (2020)
CH Colocaró	MS2	-						Huaman et.al (2020)
CH Bajo MDD	MS3	-						Huaman et.al (2020)
CH Alto MDD	MF4	-						Huaman et.al (2020)
Río Caychive	-	-						Mosquera et.al (2009)
Río Inambari	-	-						Mosquera et.al (2009)
Placeres de Madre de Dios	-	-						Hérail et al. (1991)

\* Optical microscopy  
 \*\* mesh value  
 \*\*\* watershed

Table 2. Distribution (%) by Size of Free Native Gold (Au) – Optical Microscopy of Reflected Light –BIZAlab Laboratory.

Size (µm)	Samples		Sieve N°
	DAI-02 %	CQI-04 %	
<13	0	0	>400
13-15	0	0	>400
16-23	0	0	>400
24-32	0	0	>400
33-75	18	0	400-200
76-106	0	0	200-140
>106	82	100	<140

Table 3. Mineralogical Associations of Puerto Belén and Raúl 1 Deposits

<b>Mining Concession</b>	<b>Technique</b>	<b>Dominant Minerals</b>	<b>Associated Trace Elements / Economically Significant Phases</b>	<b>Frequency and Relative Abundance</b>
<b>Puerto Belen</b>	XRF	Fe, Ti, Si, REE	Titanium (Ti), Iron (Fe), Rare Earth Elements (REE), Gold (Au)	High Fe and Ti content; moderate REE concentrations
	XRD	Ilmenite, Magnetite, Hematite, Quartz, Zircon	REE-bearing phases, Titanite	Magnetite and ilmenite abundant; zircon and hematite in lower amounts
	SEM-EDS	Gold, Ilmenite, Zircon, Magnetite	Au inclusions in magnetite; Ti and REE associated with ilmenite	Gold in fine particles; Ti and REE-rich phases in ilmenite
	Optical Microscopy	Magnetite, Hematite, Quartz, Zircon, Gold	Gold observed within magnetite grains	Gold is mostly free, but some inclusions within iron oxides
	XRF	Fe, S, Ti, Si	Sulfur (S), Iron (Fe), Titanium (Ti), Gold (Au)	High Fe and S content; moderate Ti concentrations
<b>Raul 1</b>	XRD	Magnetite, Pyrite, Goethite, Quartz, Rutile	Sulfide phases enriched in gold and titanium	Magnetite and pyrite dominant; moderate goethite and rutile
	SEM-EDS	Gold, Pyrite, Rutile, Goethite, Magnetite	Au within sulfide phases; Ti concentrated in rutile	Gold associated with pyrite and magnetite; rutile enriched in Ti
	Optical Microscopy	Pyrite, Magnetite, Goethite, Quartz, Gold	Gold visible within sulfide grains and free grains in gangue minerals	Gold found within pyrite, some as free particles